Investigation of UF membranes fouling and potentials as pre-treatment step in desalination and surface water applications

Saif Al Aani[a]

Chris J. Wright[b]

N. Hilal[a, c, *]

n.hilal@swansea.ac.uk

[a]Centre for water Advanced Technologies and Environmental Research (CWATER), College of Engineering, Swansea University, Fabian Way, Swansea SA1 8EN, UK

[b]Biomaterials, Biofouling and Biofilms Engineering Laboratory (B^{3}EL), The Systems and Process Engineering Centre (SPEC), College of Engineering, Swansea University, Fabian Way, Swansea SA1 8EN, UK

[c]College of Engineering, University of Sharjah, P.O. Box 2727, Sharjah, United Arab Emirates

*Corresponding author at: Centre for water Advanced Technologies and Environmental Research (CWATER), College of Engineering, Swansea University, Fabian Way, Swansea SA1 8EN, UK.

Abstract

The surface fouling of UF membranes used upstream as pre-treatment stage is critical for the long-term stability of the subsequent treatment stage (NF/RO membranes). In this paper, an attempt was made to probe and compare the potential of versatile UF membranes structures in terms of flux decline and selectivity, for more convenient pretreatment membranes selection. The role of polyethersulfone (PES) host polymer concentration, on the morphology and surface characteristics of asymmetric flat sheet ultrafiltration (UF) membranes, has been comprehensively investigated. Distinctly, as the casting solution viscosity decrease, a higher pore size, pore size distribution and pure water flux was observed along with lower mechanical properties and wider cross-section morphologies. However, this impact was trivial on water contact angle, surface roughness parameters and charge negativity of the membrane. To further assess the potential performance of the hand-made fabricated membranes, they were systematically evaluated against three organic model foulants with dissimilar origins; humic acid (HA) – as natural organic matters (NOM), sodium alginate (NaAlg) – as polysaccharide, and bovine serum albumin (BSA) – as protein, under different initial feed concentration and pH chemistry. A disparate fouling behavior was observed depending on the membrane characteristics and the organic model foulant used. Depending on the UF membrane cut-off used, lower MWCO membranes, PES22 (6 kDa) and PES20 (10 kDa) exhibited a negligible relative flux decline while extremely low relative flux patterns were observed in the filtration with the 100 kDa membrane (PES16), as a result of one or more pore blocking mechanisms observed.

Keywords: Pre-treatment; Desalination; Polyethersulfone membrane; PES concentration; ~~h~~Humic acid; ~~b~~Bovine serum albumin; ~~s~~Sodium alginate; ~~f~~Fouling

~~1.~~1 Introduction

UF membranes have been given a special consideration as pretreatment membranes for desalination plants via providing high quality feed water to ensure stable and reliable operation of the desalination units. In addition to remarkable potentials against much more difficult liquid environments such as industrial and municipal wastewaters. Regardless of raw water turbidity, UF membranes provide an absolute barrier to pathogens and particulates, and act as a safe guard for the RO membranes by physical separation of solids, unlike conventional pretreatment methods [1]. Thus, UF can bestow significant opportunities for the future prospects of water treatment, taking into account its cost and energy efficiency when compared with conventional separation techniques. In addition, introducing the technology enables many industries to become eco-friendlier by facilitating the recycling of waste materials and resources recovery [2].

Substantial effort has been devoted in the last few decades to fabricate synthetic polymeric membranes with desired selectivity, permeability, structure and physiochemical properties. Numerous synthetic membranes structures have been produced via a variety of techniques and synthetic materials. One of the most notable techniques is the phase inversion (PI) or phase separation (PS) technique, induced by immersion precipitation, and most of the flat sheet-polymeric membranes are made using this technique [3]. Compared to conventional techniques, PI is extremely versatile and allows high flexibility in membrane material selection, and a wide range of pore sizes (1–10,000 nm) can be obtained, as long as the system (polymer-solvent) miscibility gap is over a defined temperature and concentration range [4]. However, during the fabrication of asymmetric polymeric membranes by PI, many major and secondary variables can also be adjusted to control the overall membrane properties. The fabricated membrane morphology, mechanical strength, permeability, and selectivity are influenced by the interplay of all synthesis

parameters. One of the key factors affecting membrane characteristics and performance is the host polymer concentration used to prepare the membranes.

It is well established in the literature that membrane's structure, obtained at the end of the PI process, relies on the physio-chemical characteristics of dope casting solution. As the concentration of a dope solution changes, surface characteristics of that synthesized polymeric membrane will vary with the formation of a range of diverse complex structures, depending on the process conditions and solution composition. Indeed, this is reflected bywould reflect on the permeation characteristics, selectivity and antifouling behavior of the membrane. Particularly, a higher polymer concentration will induce the formation of a higher viscosity dope solution at the bimodal-phase separation point and form a denser structure.

Currently, membrane process sustainability is still doubted in some industrial applications and fouling of membranes represents an inherent and significant issue due to its complexity and variety [5]. According to Hilal et. alet al., membrane fouling phenomena can take place at different locations in membranes, including at both selective layer and pore walls. Internal fouling refers to the deposition and adsorption of small particles or molecules onto the pore entrances or the inside of a pore of the membrane whereas external fouling refers to the accumulation of rejected molecules upon the membrane surface [6]. These fouling mechanisms could occur at different degrees depending on the characteristics of the membrane and targeted organic molecules. For instance, the fouling behavior of porous microfiltration (MF) and ultrafiltration (UF) membranes are significantly different to those observed for seawater nanofiltration (NF) and reverse osmosis (RO) membranes.. pPore blocking is the common fouling mechanism in the MF and UF membranes while it is not considered for the NF and RO membranes. Moreover, pore blocking is suggested to be a larger contributor than cake formation in UF membrane fouling and is influenced by the surface density of membrane pores and the pore size distribution [7, 8]. Thus, understanding the contributing fouling process mechanisms is a fundamental approach to provide better means for minimizing membrane fouling and its sub-consequences, enabling the adoption of an adequate membrane separation process and operating conditions for targeted industrial applications.

Organic compounds such as humic substances, proteins, and polysaccharides in water are the most abundant foulants in UF of many industrial operations. These foulants are inherently severe for pressure-driven membranes due to their strong irreversible adsorption on the surface of the membrane, causing a dramatic decline in membrane permeation, and raise many issues regarding product quality and process cost [9]. The degree of selectivity and fouling does not only depend on membrane properties but also on the complexity of the foulants' composition, their molecular weight and the charge of organic compounds, alongside the hydrodynamic conditions and solution chemistry [10]. Solution chemistry is critical for controlling the charge and configuration of organic foulants that will influence the intramolecular and molecules-membrane interactions, and hence membrane performance [11]. More precisely, performance may differ for different solute types (charged or neutral) and shapes (globular, linear or branched solute), that have similar molecular weight- [12]. This may be the case even under the same operating conditions.

In the present research, an investigation was made into the influence of PES concentration on UF membrane morphology and surface characteristics. PES/UF membranes have been synthesized with a wide range of structures that correspond to typical commercially available UF membranes. Fouling behavior and retention efficiency tests were conducted to give a more precise and comprehensive assessment of UF membrane fouling. Three different organic model foulants (HA, BSA, and NaAlg) were applied for this comprehensive fouling assessment under a broad range of feed concentration and solution pH.

2.2 Experimental

2.1.2.1 Materials and reagents.

Polyethersulfone (PES) flakes (M.wt 75,000) were kindly donated by BASF Co. Ltd. (Germany). Polyvinylpyrrolidone (PVP 40 k), *N*-methyl-2-pyrrolidone (NMP) with ≥99% purity, polyethylene glycol PEG (600 Da-35 kDa), polyethylene oxide PEO (100 kDa), humic acid (HA, ~2-500 kDa) as natural organic matter (NOM), Sodium Alginate (NaAlg, ~12-80 kDa) from Brown algae as polysaccharide, and bovine serum albumin (BSA, ~66 kDa) as protein were all purchased from Sigma Aldrich, UK. While 200 nm carboxylated polystyrene latex as tracer particles were supplied by Polysciences Inc., PA, USA.

2.2.2.2 Membranes fabrication

Since a very low and high casting solution viscosity results in a brittle and tight membrane structure, respectively. Four asymmetric PES flat sheet membranes, with a different PES polymer weight percent (wt-%), were fabricated. Each membrane was denoted according to the membrane composition, as tabulated in Table 1. The compositions used here correspond to the range of PES concentration used in literature for producing loose to tight UF membranes.

Table 1 Composition of PES membranes.

alt-text: Table 1

Membrane ID	PES wt.%	NMP wt.%	PVP K30 wt.%
PES22	22	76	2
PES20	20	78	2
PES18	18	80	2
PES16	16	82	2

All membranes were fabricated via the classical non-induced phase separation (NIPS) technique as described elsewhere [13]. In brief, for membranes fabrication, a fixed amount (2 wt.%) of PVP K30 was dissolved in NMP using a double neck-round bottom flask. The PES flakes were then gradually added to the solution and mechanically stirred overnight at 50 °C until a homogenous, yellowish and clear solution was achieved. The casting solution was then degassed under vacuum for an hour to get rid of air bubbles. For solution casting, about 10 ml of casting solution was poured onto a glass substrate and cast at a regular shear rate (225 s^{-1}) via an automated casting knife (RK film applicator). The resultant thin film was directly placed in a DI water bath at 20 °C for precipitation. Within less than ~~two minutes~~2 min, the membrane was detached from the glass substrate indicating that the phase inversion was completed. The membranes were then repeatedly rinsed with DI water to remove residual solvent and stored wet at 4 °C until used. All membranes were cast with 200 µm clearance gap at ambient temperature and relative humidity (RH% 45 ± 5). Prior to testing, the membranes were inspected under light to make sure there was no pinholes, wrinkles or any defect that could produce a performance discrepancy.

~~2.3.~~2.3 Characterization

Pure water flux (PWF) and organic filtration experiments were conducted under a crossflow condition with an active membrane area of 12.6 cm^2 and controlled temperature of 20 ± 0.5 °C. After 30 min compaction time at 0.5 MPa, the pressure was reduced to 0.4 MPa and the DI water permeate flux recorded automatically every 1 min, using data collection software interfaced with an electronic balance. The automated software converted the permeate weight data received from the balance into a flux and recorded the values on an excel spreadsheet for previously set membrane area and time intervals. For the evaluation of UF membrane performance, the pH and concentration of the organic molecule in feed solutions were varied. After the compaction with DI water, the permeate flux (~~L~~l/m^2.h~~r~~) decline was recorded as described earlier for PWF, and the relative flux (RF) in (%) was used to express the correlation of the permeate flux to the pure water flux of the respective virgin membrane. While rejection values (R%) of the membranes were determined by the Eq~~uation~~. (1):

$$R\ (\%) = \frac{C_f}{C_p} \times 100 \quad \textbf{(1)}$$

~~w here~~Where C_p and C_f are the organic concentration in the permeate and feed solutions, respectively. The concentration of feed and permeate samples were analyzed using Total Organic Carbon analyzer (TOC-L, Shimadzu). In addition, total fouling (F_T), reversible fouling (F_{rev}) and irreversible fouling (F_{ir}) of membranes are determined as below (Eq~~uations~~s. (2) to (5)) where J_o, J_1, and J_2 are initial water flux of virgin membrane, solute flux and water flux of fouled membrane after water flushing, respectively [14]. All measurements were replicated to take into account the membrane variability.

$$F_T = F_{rev} + F_{ir} \quad \textbf{(2)}$$

$$F_T\ (\%) = \frac{J_2}{J_o} \times 100 \quad \textbf{(3)}$$

$$F_{rev}\ (\%) = \frac{J_2 - J_1}{J_o} \times 100 \quad \textbf{(4)}$$

$$F_{ir}\ (\%) = \frac{J_o - J_2}{J_o} \times 100 \quad \textbf{(5)}$$

Surface hydrophilicity/hydrophobicity of the UF membranes was evaluated via a sessile drop method using a VCAoptima contact angle instrument. 4 µl droplets of DI water were dropped onto a flat membrane~~'~~s surface, and an

image of the droplet was automatically captured to determine the contact angle measurement using VCA Optima XE software. At least ten measurements for three membranes replicates were recorded and the results were averaged.

The zeta potential (ZP) of the surface of the membrane was determined using a surface zeta potential cell (ZEN1020), as an accessory kit for the Malvern Zetasizer ZN nanoseries instrument (Malvern Instruments Ltd., Malvern, UK), along with 200 nm carboxylated polystyrene latex, as tracer particles. Membranes were cut into (5 x 3.5 mm) dimensions and attached to the sample holder using double-sided sticky tape. Tracers were then dispersed in an electrolyte solution (10 mM NaCl), and the measurements performed as a function of the pH. Finally, the electrophoretic mobility of the tracers was measured at different displacements (125, 250, 375 and 500 μm) from the membrane surface. An intercept could be extrapolated by plotting electrophoretic mobility or zeta potential of the tracers at multiple distances away from the membrane surface, and the surface zeta potential of the membrane was determined according to Equation. (6) [15].

$$\zeta\,(\text{surface}) = -\text{intercept} + \zeta\,(\text{tracing particle}) \quad \textbf{(6)}$$

The mechanical properties, including the stress/strain relationship and elastic modulus of the prepared membranes, were determined using a tensile tester instrument (Instron 1162, UK). All membranes samples were cut into a standard strap (1 cm x 4 cm) and the measurements were made at a crosshead speed of 0.5 mm/min.

Scanning electron microscopy (SEM S4800- Hitachi, Japan) was used to observe the cross-section morphology of membranes. And atomic force microscopy (AFM) imaging was used to characterize the surface roughness parameters, using a multimode AFM with a NanoScope IIIa controller (Bruker, USA).

Mean pore size and pore size distribution (PSD) of membranes were determined using a solute transport model. PEG/PEO as uncharged organic solutes with different molecular weights were used during the experiments. In all experiments, solution temperature and the transmembrane pressure were kept constant at 22 ± 0.5 °C and 4 bars, respectively. Following the compaction of membranes, a sequence of, 200 mg/l of five different molecular weight PEG solutions were passed through each membrane, for each membrane, the lowest PEG molecular weight aqueous solution was firstly introduced followed by the next higher one and so on until the highest molecular weight PEG. After each increase in PEG molecular weight, a sample from the permeate side was taken after 10 ml of permeate had passed through the membrane. Both feed and permeate concentrations were analyzed by a Total Organic Carbon analyzer (TOC-L, Shimadzu), whereas different PEG solute separation percents were calculated via Equation. (1). In addition, the probability density function was used to describe the various pore size distribution curves [16], as shown below (Equation. (7))

$$\frac{df\left(d_p\right)}{d\left(d_p\right)} = \frac{1}{d_p\,\ln\sigma_p(2\pi)^{\frac{1}{2}}}\;\exp\left(-\frac{\left(\ln d_p - \ln\mu_p\right)^2}{2\left(\ln\sigma_p\right)^2}\right) \quad \textbf{(7)}$$

where d_p, $\sigma_{p,}$ and μ_p are the diameter of pore, geometric standard deviation and mean pore size, respectively.

3.3 Results and discussions

3.1.3.1 Polymeric membranes characterization

3.1.1.3.1.1 Cross-sectional analysis by Sscanning Eelectron Mmicroscope (SEM)

The cross-sectional structure has a significant influence on a membrane's transport mechanism. SEM images of all membranes obtained from 16, 18, 20 and 22 wt% PES casting solutions show a typical asymmetric structure with clear active and supporting layer for all membranes (Fig. 1).

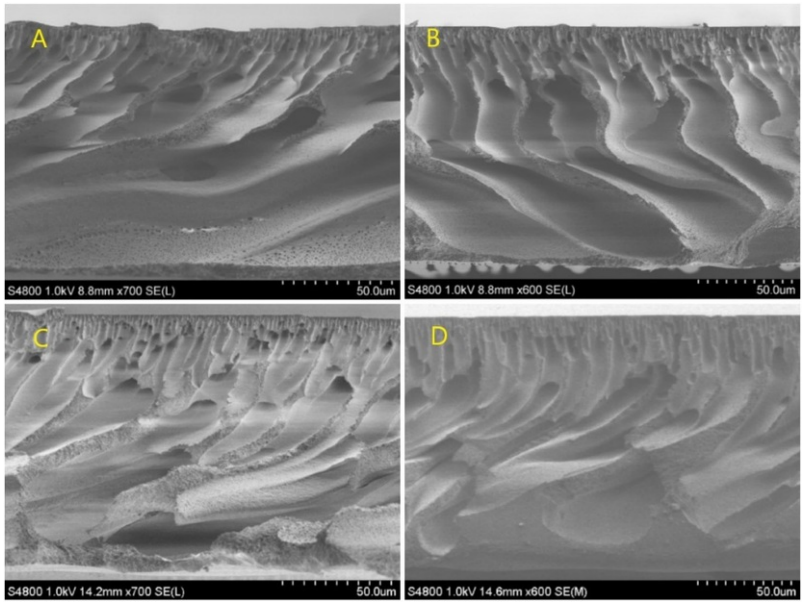

Fig. 1 SEM cross-section images for; (A) PES16, (B) PES18, (C) PES20, and (D) PES22 membrane.

alt-text: Fig. 1

Fig. 1A shows a well-developed skin layer, connected and supported by a system of wide finger-like macro-pores, as can be observed at the bottom of the PES16 membrane. This structure is most apparent for membranes fabricated with a low viscosity casting solution, where the nonsolvent exchange rate into the polymer lean phase exceeds the outward solvent diffusion rate [17]. Increasing the polymer concentration suppressed these macro-pores in the sub-layer and led to a slightly narrower finger-like structure from the top to the bottom layer of the PES18 membrane, (Fig. 1B). While PES20 and PES22 membranes, which had the highest polymer concentration, manifested the densest structure, in comparison to PES18 and PES16. This was correlated with their higher casting solution viscosity, leading to a denser membrane structure. A higher viscosity solution can hinder the solvent-nonsolvent exchange rate at the interface between the surface and the nonsolvent, producing a dense skin layer and less porous membrane [18]. Indeed, the microporous finger-like structure ~~can be~~ observed in Fig1C and D, are supported on a sponge-like structure at the bottom, especially for PES22 ~~(Fig. 1C and Fig. 1D)~~.

~~3.1.2.~~3.1.2 Surface morphology analysis by ~~A~~atomic ~~F~~force ~~M~~microscope (AFM)

AFM was used to ~~characterise~~characterize the membrane surfaces and Fig. 2 presents the 1 μm ~~x~~ × 1 μm 3D images that have been used for membrane roughness analysis. All membranes manifested a smooth surface, which is the main surface characteristic associated with PES membranes. The relationship between the PES concentration used to prepare the membranes, and the membrane roughness parameters are listed in Table 2. The presented parameters demonstrate that as the polymer wt~~.~~% decreases, a rougher membrane surface can be formed. The PES22 membrane, which was fabricated with the highest concentration had the flattest membrane surface with only 19.39 nm difference between the highest peak and lowest valley. While the R_{ms} value was 2.28 nm. A decrease in polymer concentration (PES20 membrane), induced slightly higher surface roughness parameters. The lowest PES wt~~.~~% dope solutions (PES16) resulted in the roughest surface and highest peak to valley values, 4.54 nm, and 40.18 nm, respectively. In similar research, a smoother surface topography was visualized by Rahimpour et al., in addition to a smaller pore size, a fewer porous sub-layer, and lesser finger-like pores when PES concentration increased from 14.4 wt~~.~~% to 16 wt~~.~~% [19].

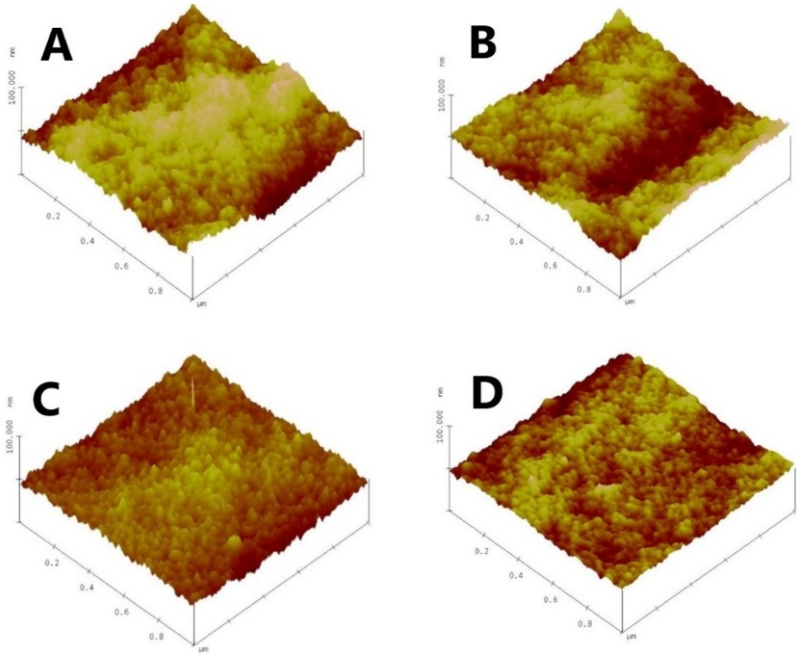

Fig. 2 (1 µm ~~x~~ × 1 µm) AFM images for; (A) PES16, (B) PES18, (C) PES20 and (D) PES22 membrane.

alt-text: Fig. 2

Table 2 Surface roughness parameters of the membranes.

alt-text: Table 2

Membrane	Polymer wt:%	R_a (nm)	R_{ms} (nm)	R_{max}
PES22	22	1.81	2.28	19.39
PES20	20	3.26	4.12	56.58
PES18	18	3.79	4.77	32.09
PES16	16	4.54	5.64	40.18

~~3.1.3.~~3.1.3 *Solute transport method*

Methods based on rejection data of solutes are proven to be more indicative methods for characterization of membrane separation performance [20]. In this work, the solute transport method was applied to estimate the mean pore size of the UF membranes, while the log normal distribution curves were used to describe the pore size distribution, more detailed description of the procedure was given by [16]. The influence of PES polymer concentration on the pore size and pore size distribution of membranes was investigated using this procedure and the data for geometric mean pore size (μ_p) and their geometric deviation (σ_p) are tabulated in Table 3. While Fig. 3 presents pore size distribution curves for the membranes. The data in Table 3 clearly demonstrates that diminishing the polymer wt:% has given rise to a bigger pore size along with a wider pore size distribution range. PES22 revealed the smallest mean pore diameter (2.17 nm) compared to the other membranes, and mean pore diameter gradually increased, with a decrease in PES concentration, from 2.93 nm, 4.41 nm and 10.79 nm for PES20, PES18, and PES16, respectively. Geometric standard deviation values were comparable and reasonable for all UF membranes. Values of σ_p associated with their corresponding µp values ranged from 1.39 ~~-~~to 1.89.

Table 3 Geometric mean pore size, standard deviation, MWCO and porosity of membranes.

alt-text: Table 3

Membrane ID	Polymer wt.%	μ_p (nm)	σ_p	MWCO
PES22	22	2.177	1.67	6 kDa
PES20	20	2.935	1.54	10 kDa
PES18	18	4.41	1.89	35 kDa
PES16	16	10.799	1.39	100 kDa

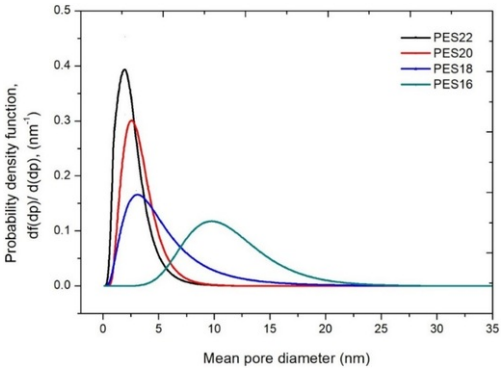

Fig. 3 Probability density function curves of UF/PES membranes.

alt-text: Fig. 3

The changes in the pore size distribution curves (Fig. 3) correlate with the pore size trend. The curves shifted to the right as the polymer weight percent was reduced for PES22 to that of PES20, which had a slightly wider distribution for the pores but with a decrease in their density. While PES18 and PES16 curves had pointedly higher shifts to the right demonstrating wider pore size distributions compared to other membranes, in addition to a lower mean pore density function. Membranes with 18 wt.% polymer or higher tended to produce a sharp cut-off in pore size while less than this critical wt.% value showed a wider pore size distribution and a diffuse cut-off. These results clearly demonstrate that the polymer wt.% in the casting solution has a significant influence on the fabricated membrane's permeation characteristics.

~~3.1.4.~~3.1.4 *Zeta potential of membranes*

Zeta potential (ZP) is known as an effective tool that can provide fundamental insights into membrane aging, separation mechanisms, membrane fouling, and cleaning. To investigate the influence of varying PES concentration on the membrane surface charge characteristics and to specify the isoelectric point (IEP) of the fabricated membranes, a new technique employing a zeta potential planar cell (ZEN1020) in conjunction with laser Doppler electrophoreses (LDE) has been applied, an extended description is presented elsewhere [21]. Fig. 4A presents a typical phase distribution, with minimal noise, obtained for the PES16 membrane at 10 mM NaCl and pH 8.4. While Fig. 4B presents the tracer particle electrophoretic mobility measured at four different distances from the membrane's surface and showing a high regression correlation (R^2 = 0.961) for the intercept of the displacement plot.

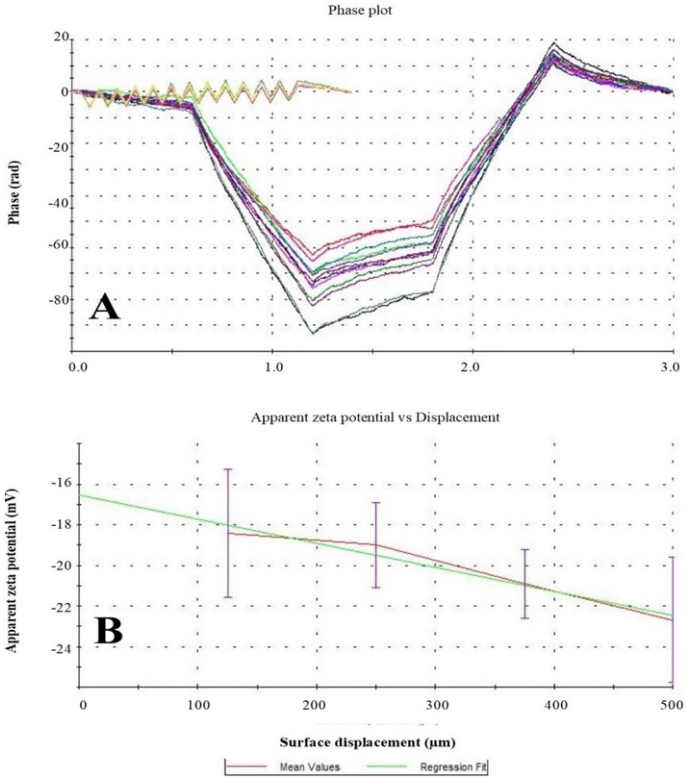

Fig. 4 (A) Measured electrophoretic mobility of tracer particles as a function of displacement from the membrane surface and (B) phase plots at four different displacements from the membrane surface.

alt-text: Fig. 4

All PES membranes were found to be negatively charged under the entire pH range investigated and the absolute values of ZP decreased with lower pH values for all UF membranes. Furthermore, no IEP could be identified, as shown in Fig. 5. The size of ZP obtained from characterizing the bare PES membranes are in line with previous research [22]. Moreover, when the host polymer concentration in the casting solution was increased, a clear pattern was evident, with an upward shift in the ZP curves. For instance, at pH 6 and 10 mM NaCl ionic strength, the smallest PES membrane concentration (PES16) had a slightly higher negative zeta potential value (−7.78 mV) than other higher concentration membranes, which were found to have a ZP of −6.5 mV, −6.81 mV and −5.4 mV for PES18, PES20 and PES22, respectively. The higher ZP measured for the membrane fabricated with a lower PES concentration could be due to the higher surface area resulting from the higher surface roughness of PES16 membranes (Table 2). The increased surface area will give rise to more functional groups on the surface of these PES membranes, which will contribute to the total net charge. The ZP measurement patterns, as a function of pH, obtained in this work were contradictory with what was observed in previous research by Sofiah et al., who reported an increase in the ZP negativity of PES membrane by almost double as the polymer concentration increased in the dope casting solution from 13 wt% to 17 wt% [17].

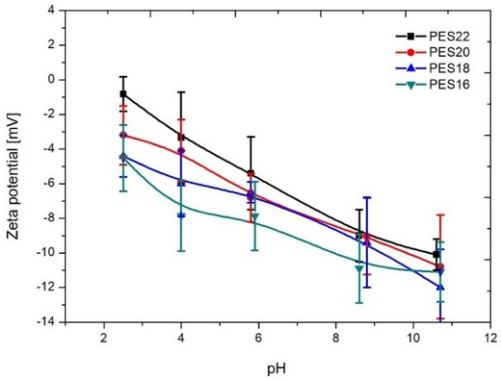

Fig. 5 Surface zeta potential profile for the UF membranes as a function of pH, determined by LDE.

alt-text: Fig. 5

~~3.1.5.~~3.1.5 Mechanical strength

The mechanical robustness of membranes can be used as an indicator to predict their performance stability under stressed conditions during industrial operations. Higher mechanical strength implies extended membrane lifespan and resistance to cleaning regimes [23]. Mechanical properties of synthesized membranes prepared with different concentrations of PES were tested. Fig. 6, presents typical stress/strain curves for the synthesized membranes. All curves had two distinctive portions comprising of an initial linear followed by a curved region that corresponded to the elastic response and inelastic response before the yield at maximum stress, respectively. The elastic modulus (Young's modulus) was calculated from the slope values of the linear portions in the stress/strain graph. Higher values of tensile strength at break, elongation and Young's modulus values were associated with the membrane fabricated from the highest PES concentration (PES22), and these values decreased with the decrease in the concentration of polymer used in membrane fabrication, as summarized in Table 4. Increasing the membrane casting solution concentration to 22 wt-% led to increase in both maximum tensile strength and elongation % by almost double their values as compared to that of 16 wt-%, while the elastic modulus was improved by 1.5 fold. The different mechanical properties of membranes are due to structural changes caused by higher viscosity casting solution, and the disappearance of big macrovoids at the bottom of membranes that are replaced by the formation of narrower finger-like structures, as discussed earlier (Section 3.1.1, Fig.1).

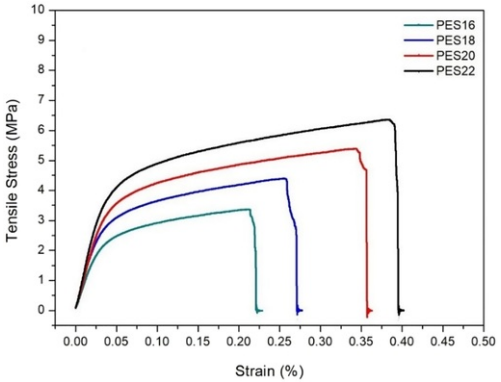

Fig. 6 Influence of dope casting solution concentration on strain-stress curves relationship of the membranes.

alt-text: Fig. 6

Table 4 Mechanical characteristics of UF membranes.

alt-text: Table 4

Membrane ID	Polymer wt-%	Tensile strength (MPa)	Elongation [%]	Young's modulus

PES22	22	6.358	39.5467	110.84
PES20	20	5.391	35.7333	100.12
PES18	18	4.394	27.2	90.596
PES16	16	3.372	22.2	73.85

~~3.1.6.~~3.1.6 Pure water flux and hydrophilicity/hydrophobicity of membranes~~.~~

A distinct inverse correlation has been unsurprisingly observed between the hydraulic permeability and polymer concentration of fabricated membranes (Fig. 7). Increasing the PES polymer concentration from 16 wt~~.~~% to 18 wt~~.~~% led to a decrease in PWF of membranes from 560 ± 30 ~~L~~l/m^2~~.~~h~~r~~ to 172 ± 12 ~~L~~l/m^2~~.~~h~~r~~, respectively. Further increase in the concentration gave rise to a further decrease in the PWF value to 48 ± 4 ~~L~~l/m^2~~.~~h~~r~~, for the PES20 membrane. While the highest PWF decline to 12 ± 0.8 ~~L~~l/m^2~~.~~h~~r~~ was associated with the highest polymer concentration (22 wt~~.~~%) for the membranes synthesized in this work.

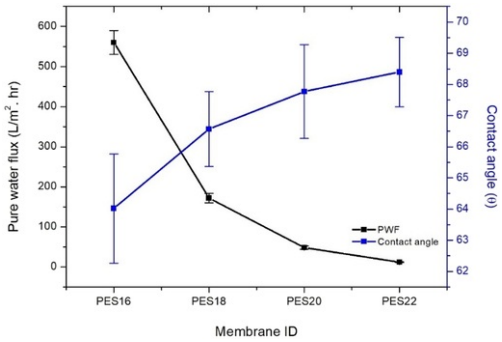

Fig. 7 ~~PWF~~Pure water flux and contact angle measurements for membranes.

alt-text: Fig. 7

This difference in PWF values between membranes was due to the different casting solution viscosities used to prepare the membranes. A higher casting solution viscosity/concentration diminishes the diffusional exchange rate during the phase inversion between the solvent and nonsolvent, where a denser skin layer with lower porosity will be formed, due to the delayed demixing. This will ultimately result in lower hydrodynamic permeability of the membranes synthesized with a higher polymer concentration.

All membranes had similar hydrophobicity as measured by contact angles (CA) (within the sixties), which were in the range of bare polyethersulfone membranes reported in the literature [24]. Only a slight decrease was observed as the polymer wt~~.~~% decreased even though all membranes were prepared with identical conditions and materials except for the polymer concentration (Fig. 7.). This could be ascribed to differences in other surface characteristics of the membranes, e.g. roughness parameters, pore size, and pore size distribution since CA values could be influenced by any change in these surface characteristics [25]. These results were in agreement with the previously reported literature [26].

~~3.2.~~3.2 Evaluation of membranes performance with organic

A lab-scale cross flow apparatus was employed to investigate the UF membranes organics retention efficiency and fouling behavior over a short filtration duration (120 min). The experiments with the chosen representative model organic (HA, BSA and NaAlg) foulants were performed at three different initial feed concentrations (20, 60 and 100 ppm) and pH (4, 7 and 10).

The influence of natural organic material (NOM) on membrane performance was investigated using HA as a model macromolecule. Experimental data showing the influence of HA solution pH on the retention coefficient and fouling behavior of the four neat PES membranes are presented in Fig. 8. As apparent in Fig. 8A, all UF membranes manifested higher than 90% retention for HA over the entire pH range tested. HA is of natural origin and not of uniform composition. According to the manufacturer, it consists of heteropolycondensates of MW's ranging from 2~~-~~ to 500 kDa, but mainly ~~–~~20~~-~~50 kDa. Therefore, a true structure cannot be given and retention data for the MWCO membranes used is indicative of the presence of low molecular weight components in the Aldrich HA. Meanwhile, the observed removal coefficients were found to be at their maximum value at neutral (pH 7) conditions for all membranes. Under highly alkaline (pH 10) feed solution, a slight decrease in the membrane retention was observed, and it was unsurprisingly found to be at the lowest value under acidic conditions (pH 4). This agreed with previous researcher on the influence of the initial feed solution pH on the retention characteristics of membranes that suggested a difference in the size and configuration of HA at dissimilar pH conditions. A possible explanation is that a high

acidic condition, induces more carboxylic groups of organic HA to be protonated, resulting in a reduction of both their macromolecular size and charge density. So, they pass more readily through membrane pores in the presence of the minimum electrostatic repulsion between membrane surfaces and organics, thus lowering the membrane rejection coefficient [27]. Interestingly, in contradiction to the trend observed in the literature, membranes with greater MWCO (PES16, PES18, and PES20), exhibited slightly higher retention compared to that of the PES22 membrane. This could be explained through the difference in membranes surface characteristics that influenced the fouling behavior of membranes to different extents. As shown in (Fig. 8B and ~~8~~C), no appreciable filtrate flux decline was detected for the low cut-off UF membranes (PES22 and PES20) under the entire pH range. This was expected since the concentration of the feed (20 ppm) and/or the short filtration time (120 min) used in the measurements was insufficient to easily foul such tight membranes under cross-flow conditions. Moreover, pore blocking and/or adsorption was insignificant due to the pore size distribution compared with the molecular cut-off distribution of the Aldrich HA. Nyström ~~et. al~~et al., also reported no flux decline when examining the fouling behavior of a 50 kDa polysulfone membrane using the same Aldrich HA [28]. Cho et al. claimed that for natural organic material fouling could be neglected for NF and low MWCO UF membrane, and the influence of concentration polarization was only significant for higher than 10 kDa MWCO membranes [29]. In contrast, a slight increase in the flux was observed at neutral condition, which could be ascribed to the increased hydrophilicity of the membrane surface imparted by binding of a proportion of the hydrophobic fraction of HA on the membrane surface, leaving the hydrophilic fraction of HA directed towards the feed solution; the fouled membrane surface possessed more hydrophilicity and negativity [30]. In the present research, the relative flux decline was more significant for the PES18 membrane, especially at acidic conditions. However, a drastically reduced relative flux was associated with the bigger pore size membrane (PES16), (Fig. 8D and ~~8~~E). This discrepancy in fouling behavior at the different membrane structures belongs to the different mechanisms contributing to the total fouling of the membranes. For instance, the initial rapid irreversible fouling that took place at the PES16 membrane, was mainly caused by adsorption of HA species inside the membrane pores and between the ridge-valley structure of the surface. Progressively, these adsorbed HA molecules act as initiation sites for further HA deposition to develop the cake layer. The hydrophobic PES16 membrane had a high pore size distribution range corresponding to a significant size fraction of the HA, thus a spontaneous complete pore blocking and/or narrowing mechanisms may have produced a smaller pore size distribution, which may explain the slightly higher retention of the PES16 as compared to that of the PES22 membrane. A similar conclusion was reached by Yuan and AL Zydney who identified that the HA retention coefficient of a membrane with a pore size of 0.16 μm became greater than the retention obtained with membranes with much smaller 100 kDa and 300 kD pores, after about 50 ~~minutes~~min of filtration [31].

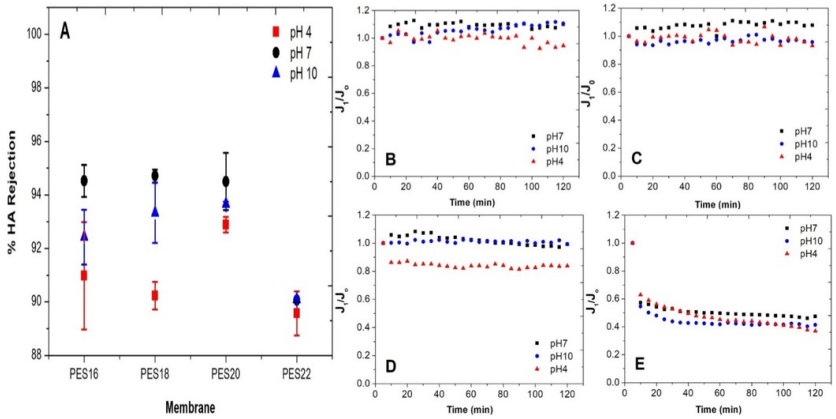

Fig. 8 Influence of solution pH on HA rejection coefficients (A), and fouling behavior of (B) PES22, (C) PES20, (D) PES18, and (E) PES16 membrane.

alt-text: Fig. 8

The influence of HA initial feed concentration on the rejection coefficients has indicated a slight increase in removal efficiency of the membranes as the HA initial feed concentration increases from 20 to 100 ppm, Fig. 9A. These coefficients were comparable in size (within 94-96%) except that of the 6 kDa membrane (PES22), which manifested a slightly lower value than other membranes, mainly at the lower feed concentration (20 ppm). When the initial feed concentration increased the influence of reversible concentration polarization was becoming more obvious as demonstrated by the improved retentive coefficients of the PES22 membrane at high concentrations. Yuan and Zydney claimed that a highly concentrated HA feed solution induces a considerable concentration polarization to take place at membranes as a consequence of the concentration-dependence of the osmotic pressure [31]. The magnitude of the relative flux patterns of the membranes is presented in (Fig. 9B~~-9~~-E). The PES16 membrane experienced a further flux decline, mainly when the higher (60 and 100 ppm) initial feed concentrations were introduced. This could be due to thicker cake layer formation at the surface, that reduces the permeability characteristics of membranes and enhances their retention.

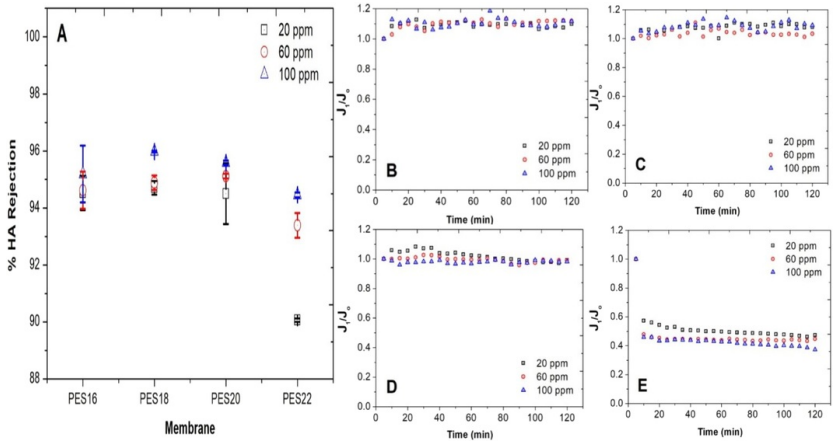

Fig. 9 Influence of solution initial feed concentration on HA rejection coefficients (A), and fouling behavior of (B) PES22, (C) PES20, (D) PES18, and (E) PES16 membrane.

alt-text: Fig. 9

The assessment of the UF membranes performance against a polysaccharide organic model was carried out using individual NaAlg solutions, Fig. 10A clearly shows the removal coefficients of membranes for different feed solution chemistry (pH) of NaAlg. Membranes behaved similarly to the trend observed for the NOM filtration, but with greater rejection magnitudes. These membranes retention coefficients were maintained as high as ~96–100%, with the smallest retentions ascribed to the PES22 membrane. On the other hand, the relative flux curves presented in (Fig. 10B and ~~10~~C) indicated that no perceivable flux decline was associated with NaAlg filtration for both PES22 and PES20 membranes. This was attributed to the insufficient feed concentration and filtration time adopted to foul these membranes; also observed for the HA filtration tests earlier in this section. In addition, the NaAlg had a greater molar mass distribution that was unable to penetrate such low cut-off membranes. For the higher MWCO PES18 membrane, a slight flux decline can be observed at the initial filtration stage suggesting that pore blocking and narrowing occurred. This was followed by a progressively increased decline without any sign of reaching the quasi-steady-state flux, Fig. 10D. The PES16 membrane manifested a prompt and a severe relative flux decline mainly at acidic conditions, Fig. 10E. The lower retention and the higher flux decline magnitudes, observed at low pH, are suggested to be induced by the solution pH and its influence on the molecular size of the polysaccharide, as acidic conditions can influence not only the structure of NaAlg molecules but also their electrostatic repulsion with the membrane surface [32]. The lower intramolecular electrostatic interactions resulting from the protonation of the carboxylic groups of the alginates would produce smaller sized NaAlg molecules [33]. Indeed, this would facilitate the passage of the resized molecules through the membrane pores and encourage their tendency to form more aggregates at low pH. The observed relative flux of the UF membranes with individual NaAlg solutions was more detrimental than the HA fouling under identical experimental conditions and was strongly dependent on the membranes cut-off used. This was attributed to the gel-forming nature of alginate that has a greater intermolecular adhesion of the NaAlg-gel network along with their larger molecular size compared to the HA might also induce the formation of a thicker fouling layer [11].

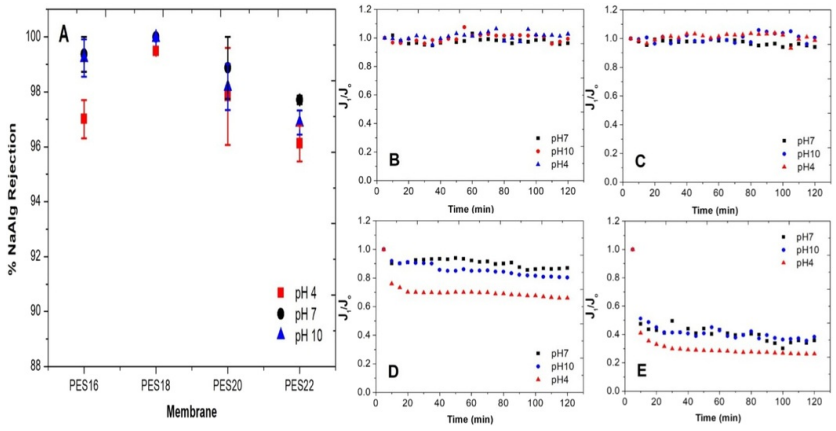

Fig. 10 Influence of solution pH on NaAlg rejection coefficients (A), and fouling behavior of (B) PES22, (C) PES20, (D) PES18, and (E) PES16 membrane.

alt-text: Fig. 10

To further assess the scope of polysaccharide retention and adsorptive fouling on UF membranes, three concentrations of NaAlg were used as a feed. As shown in Fig. 11, all membranes had a very small rise in their retention coefficients and relative flux reduction with increasing initial feed concentration. This suggested that alginate adsorption, inside the membrane pores and on the surface, has readily taken place, even at the low alginate concentration (20 ppm), especially on the 100 kDa membrane, and to a lower extent on the 35 kDa membrane. Whereas, at 100 ppm concentration, some flux reduction for the PES20 was observed but not for the PES22 membrane. Disagreement can be seen between these results and previous research reported by Susanto et al., who found that a 10 kDa UF membrane had fouling behavior that was very influenced by the NaAlg concentration [32]. This difference is likely associated with the difference in membrane properties, experimental conditions and feed characteristics used in the measurements.

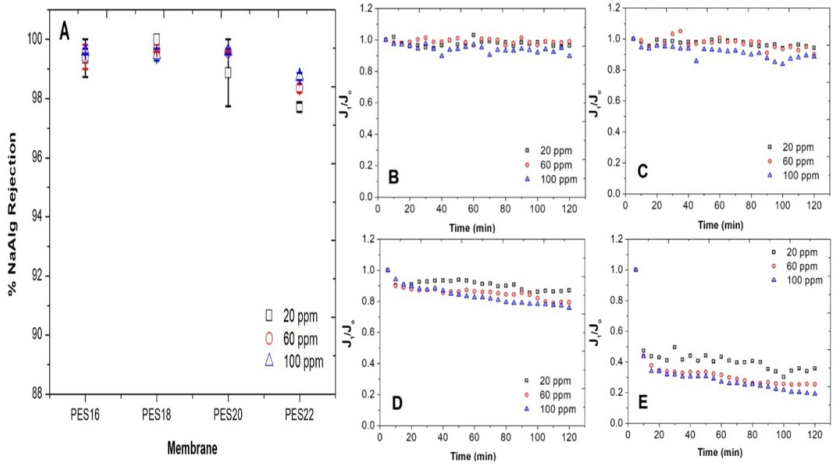

Fig. 11 Influence of solution initial feed concentration on NaAlg rejection coefficients (A), and fouling behavior of (B) PES22, (C) PES20, (D) PES18, and (E) PES16 membrane.

alt-text: Fig. 11

The protein retention and fouling behavior were also investigated in the filtration of the UF membranes using BSA. Similar to the retention trend observed with other model organics, BSA retention was found to be influenced by the feed solution chemistry (pH), where lower rejection values were observed at acidic conditions for all membranes, Fig. 12A. It should be noted that retention and permeate flux behavior in UF membranes can be related to different mechanisms, for instance, different experimental conditions may result in different fouling mechanisms or protein characteristics [34]. Depending on the pore size distribution of the membrane applied for BSA filtration, uneven contribution for protein fouling mechanisms was observed on the membranes. As previously observed with HA and NaAlg filtration, PES20 and PES22 did not exhibit apparent relative flux declines due to the insufficient concentration and filtration time required to foul the membranes with BSA. In addition, the narrow pore distribution of these membranes prevented pore blocking, Fig. 12B and ~~12~~C. In fact, the membrane fouling process with protein is complex due to the multiple interactions between membrane surfaces and protein molecules, and intramolecular interactions of the protein. The fouling can be interpreted as a two-stage process [35]. According to Huisman, BSA-membrane hydrophobic interactions are dominant at the initial stage of filtration, while the high fouling regime that dictates the overall performance, was attributed to protein-protein interactions [34]. For PES18 membrane, the relative flux pattern is more pronounced, particularly under acidic conditions. The initial hydrophobic interactions between the protein and membrane were marginal and did not cause any tangible fouling before the first 40 ~~minutes~~min of filtration. While slight flux decline commenced after 40 ~~minutes~~min of filtration demonstrating the dominant role of solute-solute electrostatic interactions on the performance of the membrane, Fig. 11D. This can be explained as follow; at pH below the IEP point of BSA, the protein molecules possess positive charges while the membrane continued to have a negative zeta potential over the entire pH range, as indicated in Section 3.1.4. At this point, the electrostatic repulsion between BSA and the membrane surface was significantly reduced and the membrane surface acquired the BSA electrostatic charge as a result of adsorption, leading to a faster deposition rate on the surface of the fouled membrane. For the large MWCO membranes (PES16), the relative flux during BSA filtration manifested only small decline during the very first minutes of the filtration experiment, at neutral or alkaline feed solution condition, Fig. 12E. This was significantly different to what was observed during the HA and NaAlg filtration utilizing the same membrane, this reduction in relative permeate flux progressed gradually without reaching any steady-state after 120 ~~minutes~~min of filtration. Arguably, a simultaneous BSA adsorption could have occurred within the pores and at the membrane's surface, during the initial 10 min stage, due to the wide pore size range of the membrane. Next, as the filtration proceeds, an accumulative adsorption of BSA-BSA fouled membrane will continue to build up a thicker layer of protein on the initial monolayer. The flux decline behavior was even more severe in the acidic condition,

which was facilitated by the weak protein-membrane interactions at low pH [36]. Another possible explanation for the lower relative flux, in this case, is that high level of protein denaturation that was induced at acidic conditions, which would consequently form aggregations at pH below the IEP [37].

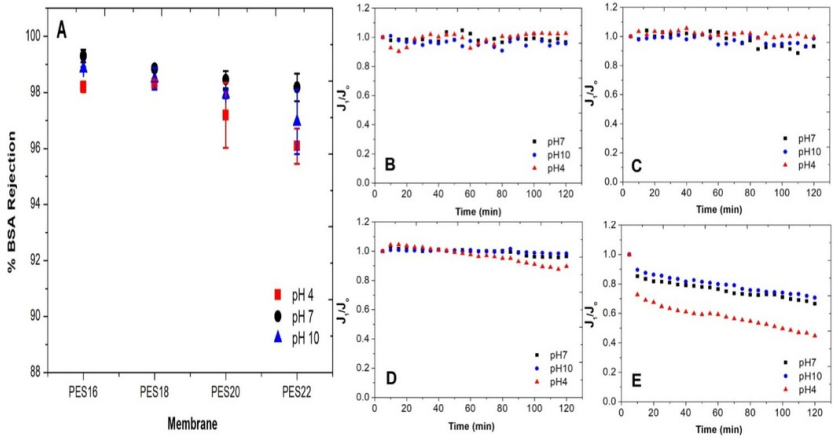

Fig. 12 Influence of solution ~~initial feed concentration~~pH on BSA rejection coefficients (A), and fouling behavior of (B) PES22, (C) PES20, (D) PES18, and (E) PES16 membrane.

alt-text: Fig. 12

In regard to the influence of BSA concentration on the retention of the membranes, Fig. 13A indicated that all membranes maintained high rejection characteristics (98–99.5%) to BSA, with a very slight improvement in retention coefficients of membranes as the initial feed concentration increased. While the relative flux decline was only significant for membranes with wide porous structure (PES18 and PES16), Fig. 13B~~-13~~E. The reason behind this flux reduction was because of a higher mass transfer coefficient at the higher concentration and a thicker cake layer would appear earlier on the surface of membranes.

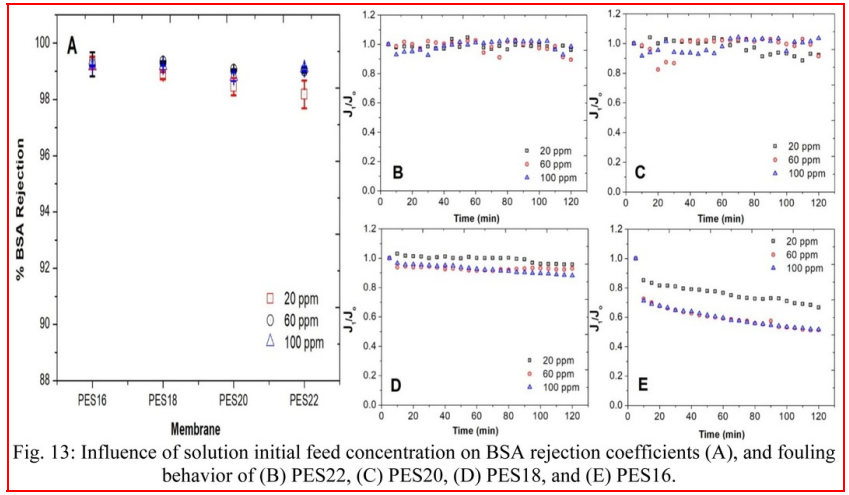

Fig. 13: Influence of solution initial feed concentration on BSA rejection coefficients (A), and fouling behavior of (B) PES22, (C) PES20, (D) PES18, and (E) PES16.

Fig. 13 Influence of solution initial feed concentration on BSA rejection coefficients (A), and fouling behavior of (B) PES22, (C) PES20, (D) PES18, and (E) PES16 membrane.

alt-text: Fig. 13

PWF measurements after back-flushing indicated that despite the NaAlg manifested higher relative flux decline, it was mostly recoverable. This was opposite to that observed with HA and BSA, which showed significant irreversible flux, mainly for wide cut-off membranes. Data of total, reversible and irreversible fouling in membranes as a function of pH and concentration are presented in ~~Table~~ Tables 5 and ~~Table~~ 6. As shown in the tables, the tide PES22

and PES20 exhibited negative fouling parameters with HA filtration under neutral and alkaline conditions, while they were marginally fouled with other organic foulants. The effect of solution chemistry and initial concentration commenced being more obvious with protein and polysaccharide filtration using the 35 kDa (PES18 membrane). The effects of the latter forms of fouling are mostly reversed by backwashing. The most severe fouling was associated with the PES16 membrane at acidic conditions, as illustrated earlier. About 63, 73 and 55 % reduction in the original flux of the PES16 membrane was observed for HA, NaAlg, and BSA, respectively. Almost 64 % of this flux decline was recovered when using the alginate while only 9 and 12 % could be restored when using HA and BSA for the same conditions.

Table 5 Total, reversible and irreversible fouling data of membranes, as a function of initial feed solution pH.

alt-text: Table 5

	PES22			PES20			PES18			PES16		
	pH 4	pH 7	pH 10	pH 4	pH 7	pH 10	pH 4	pH 7	pH 10	pH 4	pH 7	pH 10
HA												
F_T	5.993	−9.342	−8.094	4.854	−7.71	3.373	15.61	1.002	−0.97	63.41	53.83	57.719
F_{Rev}	8.508	0.105	−2.253	4.358	−5.83	2.682	4.133	0.733	1.245	9.2841	5.464	8.7039
F_{Irr}	−2.52	−9.447	−5.841	0.496	−1.88	0.691	11.48	0.269	−2.22	54.126	48.37	49.015
NaAlg												
F_T	4.188	1.521	4.22	3.886	4.414	2.659	34.89	13.17	20.24	73.471	62.41	60.641
F_{Rev}	1.742	0.181	1.807	3.676	3.729	2.071	30.84	6.955	17.52	63.851	51.1	52.316
F_{Irr}	2.446	1.34	2.413	0.21	0.685	0.588	4.049	6.212	2.727	9.62	11.31	8.3257
BSA												
F_T	3.636	4.211	4.401	3.631	2.222	2.453	11.96	4.67	2.095	55.656	33.61	29.428
F_{Rev}	1.571	2.456	1.738	2.46	0.461	0.231	1.145	1.141	0.257	12.158	8.745	5.779
F_{Irr}	2.065	1.755	2.663	1.171	1.76	2.222	10.81	3.529	1.838	43.497	24.87	23.649

Table 6 Total, reversible and irreversible fouling data of membranes, as a function of initial feed concentration.

alt-text: Table 6

	PES22			PES20			PES18			PES16		
	20 ppm	60 ppm	100 ppm	20 ppm	60 ppm	100 ppm	20 ppm	60 ppm	100 ppm	20 ppm	60 ppm	100 ppm
HA												
F_T	−9.34	−9.945	−10.51	−7.708	−3.69	−8.45	1.002	1.87	2.086	53.829	55.73	60.781
F_{Rev}	0.105	−5.701	−5.226	−5.83	−2.96	−7.51	0.733	0.144	0.454	5.4636	6.72	13.636
F_{Irr}	−9.45	−4.243	−5.288	−1.878	−0.74	−0.94	0.269	1.726	1.632	48.366	49.01	47.144
NaAlg												
F_T	1.521	2.994	9.408	4.414	4.743	10	13.17	20.61	24.85	62.408	75.02	78.529

F_{Rev}	0.181	2.283	3.188	3.729	4.117	7.2	6.955	19.05	23.41	51.097	66.99	70.41
F_{Irr}	1.34	0.71	6.22	0.685	0.626	2.8	6.212	1.562	1.442	11.311	8.022	8.1197
BSA												
F_T	4.211	13.53	10.4	4.571	3.861	2.903	4.67	9.576	12.06	33.613	49.06	48.578
F_{Rev}	2.456	10.54	8.14	2.811	2.683	2.107	1.141	4.314	2.526	8.7454	8.357	17.23
F_{Irr}	1.755	2.988	2.26	1.76	1.179	0.796	3.529	5.262	9.533	24.867	40.7	31.348

4.4 Conclusions

Asymmetric UF membranes with versatile morphologies and characteristics have been produced via the classical non-induced phase separation. As a result of variation in the viscosity of casting solutions, significant differences in the PWF, PS and PSD, cross-section morphology and mechanical strength were observed, while this influence was insignificant for roughness parameters, water contact angle and surface charges of the membranes. A comparison was also made to provide valuable insight into details of organic molecules-membrane interactions to better understand the role of membranes surface properties when challenged with the natural organic matter, polysaccharides and proteins. Despite the large variation in membranes surface properties, the differences in their rejection coefficients were not significant, as the different MWCO characteristics obtained are compromised by different fouling mechanisms. In addition, it should be noted that the influence of surface roughness parameters, hydrophilicity and surface charge cannot be considered in the comparison since these measurements were similar for all membranes. When the fouling studies were considered, the relative flux decline was negligible for the low MWCO membranes, PES22 and PES20, within the short filtration duration of 120 min used in this research. In contrast, extremely low relative flux patterns were observed in the filtration with the 100 kDa membrane (PES16). Adsorption effects were small for the low cut-off PES22 (6 kDa) and PES20 (10 kDa) membranes with all organic models used. While they were significant for fouling at the PES18 (35 kDa) membrane. In contrast, the larger pore (PES16) membranes experienced an instantaneous adsorption resulting in a considerable relative flux decline, mainly in acidic conditions and highly concentrated feed solutions. Finally, although NaAlg manifested higher relative flux decline, it was mostly recoverable compared to HA and BSA filtration, which showed significant irreversible flux, mainly for the 100 kDa membranes.

Abbreviations

alt-text: Unlabelled Table

Nomenclatures	Description
µm	Micrometre
μ_p	Mean pore size
3D	Three dimensions
AFM	Atomic force microscopy
BSA	Bovine serum albumin
CA	Contact angles
C_f	concentration in the feed solutions
C_p	concentration in the permeate solutions
DI	Deionized water
d_p	Diameter of pore
F_{ir}	Irreversible fouling
F_{rev}	Reversible fouling
F_T	Total fouling

HA	Humic acid
IEP	Isoelectric point
J_1	Solute flux
J_2	Water flux of fouled membrane after water flushing
J_o	Initial water flux of virgin membrane
kDa	Kilo Dalton
LDE	Laser Doppler electrophoreses
MF	Microfiltration
mM	Millimolar
MPa	Mega pascal
mV	Millivolt
MWCO	Molecular weight cut-off
NaAlg	Sodium alginate
NaCl	Sodium chloride
NF	Nanofiltration
nm	Nanometre
NMP	*N*-methyl-2-pyrrolidone
NOM	Natural organic matters
PEG	Polyethylene glycol
PEO	Polyethylene oxide
PES	Polyethersulfone
PI	phase inversion
ppm	Part per million
PS	phase separation
PSD	Pore size distribution
PVP	Polyvinylpyrrolidone
PWF	Pure water flux
R%	Rejection percent
R^2	Regression correlation
R_a	Root average arithmetic roughness
RF	Relative flux
RH	Relative humidity

R_{max}	Ridge to valley distance
R_{ms}	Root mean square roughness
RO	Reverse osmosis
SEM	Scanning electron microscopy
TOC	Total Organic Carbon
UF	Ultrafiltration
wt-%	Weight percent
ZP	Zeta potential
ξ	Zeta potential
σ_p	Geometric standard deviation

Acknowledgment

The authors wish to thank The Higher Committee for Education Development in Iraq (HCED) for providing a Ph.D. scholarship to Saif Al Aani.

References

[1] P.H. Wolf, S. Siverns and S. Monti, UF membranes for RO desalination pretreatment, *Desalination* **182**, 2005, 293–300.

[2] R. Rohani, M. Hyland and D. Patterson, A refined one-filtration method for aqueous based nanofiltration and ultrafiltration membrane molecular weight cut-off determination using polyethylene glycols, ~~*Journal of membrane science*~~*J. Membr. Sci.* **382**, 2011, 278–290.

[3] C. Zhao, J. Xue, F. Ran and S. Sun, Modification of polyethersulfone membranes – ~~A~~a review of methods, ~~*Progress in Materials Science*~~*Prog. Mater. Sci.* **58**, 2013, 76–150.

[4] N. Hilal, A.F. Ismail and C. Wright, Membrane Fabrication, 2015, CRC Press.

[5] A.F. Ismail, M. Padaki, N. Hilal, T. Matsuura and W.J. Lau, Thin film composite membrane—~~R~~recent development and future potential, *Desalination* **356**, 2015, 140–148.

[6] N. Hilal, O.O. Ogunbiyi, N.J. Miles and R. Nigmatullin, Methods ~~E~~employed for ~~C~~control of ~~F~~fouling in MF and UF ~~M~~membranes: ~~A~~a ~~C~~comprehensive ~~R~~review, ~~*Separation Science and Technology*~~*Sep. Sci. Technol.* **40**, 2005, 1957–2005.

[7] F. Wang and V.V. Tarabara, Pore blocking mechanisms during early stages of membrane fouling by colloids, ~~*Journal of colloid and interface science*~~*J. Colloid Interface Sci.* **328**, 2008, 464–469.

[8] W.R. Bowen, N. Hilal, R.W. Lovitt and P.M. Williams, Atomic ~~F~~force ~~M~~microscope ~~S~~studies of ~~M~~membranes: ~~S~~surface ~~P~~pore ~~S~~structures of Diaflo ~~U~~ultrafiltration ~~M~~membranes, ~~*Journal of Colloid and Interface Science*~~*J. Colloid Interface Sci.* **180**, 1996, 350–359.

[9] W.L. Ang, A.W. Mohammad, N. Hilal and C.P. Leo, A review on the applicability of integrated/hybrid membrane processes in water treatment and desalination plants, *Desalination* **363**, 2015, 2–18.

[10] Y.P. Lim and A.W. Mohammad, Effect of solution chemistry on flux decline during high concentration protein ultrafiltration through a hydrophilic membrane, ~~*Chemical Engineering Journa,*~~*Chem. Eng. J.* **159**, 2010, 91–97.

[11] M.A. Zazouli, S. Nasseri and M. Ulbricht, Fouling effects of humic and alginic acids in nanofiltration and influence of solution composition, *Desalination* **250**, 2010, 688–692.

[12] M. Mulder, Basic Principles of Membrane Technology, 1996, Springer.

[13] S. Al Aani, V. Gomez, C.J. Wright and N. Hilal, Fabrication of antibacterial mixed matrix nanocomposite membranes using hybrid nanostructure of silver coated multi-walled carbon nanotubes, ~~*Chemical Engineering Journa,*~~*Chem. Eng. J.* 2017.

[14] V. Vatanpour, S.S. Madaeni, R. Moradian, S. Zinadini and B. Astinchap, Fabrication and characterization of novel antifouling nanofiltration membrane prepared from oxidized multiwalled carbon nanotube/polyethersulfone nanocomposite, ~~*Journal of Membrane Science*~~*J. Membr. Sci.* **375**, 2011, 284–294.

[15] J.C.W. Corbett, F. McNeil-Watson, R.O. Jack and M. Howarth, Measuring surface zeta potential using phase analysis light scattering in a simple dip cell arrangement, ~~*Colloids and Surfaces A: Physicochemical and Engineering Aspects*~~*Colloids Surf. A Physicochem. Eng. Asp.* **396**, 2012, 169–176.

[16] S. Singh, K. Khulbe, T. Matsuura and P. Ramamurthy, Membrane characterization by solute transport and atomic force microscopy, ~~*Journal of Membrane Science*~~*J. Membr. Sci.* **142**, 1998, 111–127.

[17] H. Sofiah, A. Nora'aini and M. Marinah, The ~~I~~influence of ~~P~~polymer ~~C~~concentration on ~~P~~performance and ~~M~~morphology of ~~A~~asymmetric ~~U~~ultrafiltration ~~M~~membrane for ~~L~~lysozyme ~~S~~separation, *J. Appl. Sci.* **10**, 2010, 3325–3330.

[18] A. Rahimpour, M. Jahanshahi, S. Khalili, A. Mollahosseini, A. Zirepour and B. Rajaeian, Novel functionalized carbon nanotubes for improving the surface properties and performance of polyethersulfone (PES) membrane, *Desalination* **286**, 2012, 99–107.

[19] A. Rahimpour, S.S. Madaeni, M. Jahanshahi, Y. Mansourpanah and N. Mortazavian, Development of high performance nano-porous polyethersulfone ultrafiltration membranes with hydrophilic surface and superior antifouling properties, ~~*Applied Surface Science*~~*Appl. Surf. Sci.* **255**, 2009, 9166–9173.

[20] E. Kang, Y. Lee, K. Chon and J. Cho, Effects of hydrodynamic conditions (diffusion vs. convection) and solution chemistry on effective molecular weight cut-off of negatively charged nanofiltration membranes, *Desalination* **352**, 2014, 136–141.

[21] T.E. Thomas, S.A. Aani, D.L. Oatley-Radcliffe, P.M. Williams and N. Hilal, Laser Doppler ~~E~~electrophoresis and electro-osmotic flow mapping: ~~A~~a novel methodology for the determination of membrane surface zeta potential, ~~*Journal of Membrane Science*~~*J. Membr. Sci.* **523**, 2017, 524–532.

[22] C. Liu, L. Shi and R. Wang, Enhanced hollow fiber membrane performance via semi-dynamic layer-by-layer polyelectrolyte inner surface deposition for nanofiltration and forward osmosis applications, ~~*Reactive and Functional Polymers*~~*React. Funct. Polym.* **86**, 2015, 154–160.

[23] L.C. Powell, N. Hilal and C.J. Wright, Atomic force microscopy study of the biofouling and mechanical properties of virgin and industrially fouled reverse osmosis membranes, *Desalination* **404**, 2017, 313–321.

[24] A. Rahimpour, M. Jahanshahi, N. Mortazavian, S.S. Madaeni and Y. Mansourpanah, Preparation and characterization of asymmetric polyethersulfone and thin-film composite polyamide nanofiltration membranes for water softening, ~~*Applied Surface Science*~~*Appl. Surf. Sci.* **256**, 2010, 1657–1663.

[25] D. Rana and T. Matsuura, Surface modifications for antifouling membranes, ~~*Chemical reviews*~~*Chem. Rev.* **110**, 2010, 2448–2471.

[26] S. Balta, A. Sotto, P. Luis, L. Benea, B. Van der Bruggen and J. Kim, A new outlook on membrane enhancement with nanoparticles: ~~T~~the alternative of ZnO, ~~*Journal of Membrane Science*~~*J. Membr. Sci.* **389**, 2012, 155–161.

[27] S. Hong and M. Elimelech, Chemical and physical aspects of natural organic matter (NOM) fouling of nanofiltration membranes, ~~*Journal of membrane science*~~*J. Membr. Sci.* **132**, 1997, 159–181.

[28] M. Nyström, K. Ruohomäki and L. Kaipia, Humic acid as a fouling agent in filtration, *Desalination* **106**, 1996, 79–87.

[29] J. Cho, G. Amy and J. Pellegrino, Membrane filtration of natural organic matter: initial comparison of rejection and flux decline characteristics with ultrafiltration and nanofiltration membranes, ~~*Water Research*~~*Water Res.* **33**, 1999, 2517–2526.

[30] M. Mänttäri, L. Puro, J. Nuortila-Jokinen and M. Nyström, Fouling effects of polysaccharides and humic acid in nanofiltration, ~~*Journal of Membrane Science*~~*J. Membr. Sci.* **165**, 2000, 1–17.

[31] W. Yuan and A.L. Zydney, Humic acid fouling during ultrafiltration, *Environ. Sci. Technol.* **34**, 2000, 5043–5050.

[32] H. Susanto, H. Arafat, E.M. Janssen and M. Ulbricht, Ultrafiltration of polysaccharide–protein mixtures: elucidation of fouling mechanisms and fouling control by membrane surface modification, ~~*Separation and Purification Technology*~~*Sep. Purif. Technol.* **63**, 2008, 558–565.

[33] S.K. Rhee and A. Steinbuchel, Polysaccharides and ~~þ~~Polyamides in the ~~f~~Food ~~I~~Industry: ~~þ~~Properties, ~~þ~~Production, and ~~þ~~Patents, Wiley-Vch2005.

[34] I.H. Huisman, P. Prádanos and A. Hernández, The effect of protein–protein and protein–membrane interactions on membrane fouling in ultrafiltration, ~~*Journal of membrane science*~~*J. Membr. Sci.* **179**, 2000, 79–90.

[35] H. Mo, K.G. Tay and H.Y. Ng, Fouling of reverse osmosis membrane by protein (BSA): effects of pH, calcium, magnesium, ionic strength and temperature, ~~*Journal of Membrane Science*~~*J. Membr. Sci.* **315**, 2008, 28–35.

[36] Q. Li, Z. Xu and I. Pinnau, Fouling of reverse osmosis membranes by biopolymers in wastewater secondary effluent: ~~R~~role of membrane surface properties and initial permeate flux, ~~*Journal of Membrane Science*~~*J. Membr. Sci.* **290**, 2007, 173–181.

[37] F. Pincet, E. Perez and G. Belfort, Do denatured proteins behave like polymers?, *Macromolecules* **27**, 1994, 3424–3425.

Highlights

- Applications of UF as pretreatment membrane in desalination~~.~~
- Role of PES concentration on UF membranes fouling behavior~~.~~
- Fouling behavior of humic acid, sodium alginate and bovine serum albumin in UF membranes~~.~~
- Organic models~~'~~ fouling mechanisms in polymeric membranes~~.~~
- Influence of PES concentration on morphology and surface characteristics of polymeric membranes~~.~~

Queries and Answers

Query:

Kindly check the layout and presentation of data in Tables 5 and 6 if correct and amend as necessary.

Answer: Table 5 is fine. but, please make sure that table 6 will fit the page (it seems bigger than the width of the page).

Query:

Your article is registered as a regular item and is being processed for inclusion in a regular issue of the journal. If this is NOT correct and your article belongs to a Special Issue/Collection please contact j.rakeshkumar@elsevier.com immediately prior to returning your corrections.

Answer: Yes

Query:

Please confirm that given names and surnames have been identified correctly and are presented in the desired order, and please carefully verify the spelling of all authors' names.

Answer: Yes

Query:

The author names have been tagged as given names and surnames (surnames are highlighted in teal color). Please confirm if they have been identified correctly.

Answer: Yes

Query:

Both the lowercase Latin letter “l” and the uppercase Latin letter “L” are used to represent the unit “liter” or its variations (e.g., milliliter, microliter) in the text. For consistency, kindly modify these occurrences so that only one format is used throughout the article.

Answer: Ok. done

Query:

Please provide the volume number and page range for the bibliography in Ref. [13].

Answer: 326, 2017, 721-736.